Eur. Phys. J. Spec. Top. (2022) 231:4167–4171
https://doi.org/10.1140/epjs/s11734-022-00574-x

THE EUROPEAN PHYSICAL JOURNAL SPECIAL TOPICS

Regular Article

Structural defects effect in fine-grained $MgAl_2O_4$ sintered ceramics: optical and RPE properties as function of microstructure

Hugo Spiridigliozzi[1,a], Silvana Mercone[2], Guillaume Lang[3], Eduard Feldbach[4], Andrei Kanaev[1], and Frédéric Schœnstein[1]

[1] LSPM UPR 3407, CNRS, Université Sorbonne Paris Nord, 93430 Villetaneuse, France
[2] GREMAN UMR7347, CNRS, Université de Tours, 37200 Tours, France
[3] LPEM, ESPCI Paris, Université PSL, Sorbonne Université, CNRS, 75005 Paris, France
[4] Institute of Physics, University of Tartu, 50411 Tartu, Estonia

Received 4 February 2022 / Accepted 9 April 2022 / Published online 17 April 2022

Abstract Transparent sintered ceramics of spinel oxides compounds have attracted a lot of attention due to their expected structural stability in extreme environments. In this work, the evolution of structural defects was observed in fine-grain transparent $MgAl_2O_4$ ceramics following consolidation of spinel powders via Spark Plasma Sintering and heat treatment under air. A dark discoloration due to a carbon contamination and partial reduction during the sintering process was suppressed via post-annealing under air. The correlated EPR and cathodoluminescence analyses showed significance of the Mn^{4+} ions reduction after consolidation of powders.

1 Introduction

Transparent ceramics based on spinel oxides has the advantage, compared to the glass, of being harder and stronger and to provide a better protection against impact, sand and erosion. Besides from spinel powder, it is possible to generate a transparent sheet by using a heat press and to obtain customized shaped transparent objects. This kind of technology could prove to be practical for military equipment (shield, armored windshield, head-up display helmet), it could also find an application in consumer electronics, in particular for smartphones and connected watches, thus making their screen unbreakable. Optically transparent $MgAl_2O_4$ spinel (MAO) ceramics with fine microstructures can be interesting for application in optical windows under extreme environment (e.g. nuclear powerplant) [1,2]. In fact MAO ceramics exhibit very good optical properties, with a theoretical transmittance of 87% between 200 and 6000 nm wavelength, as well as a high hardness up to 16 GPa [3,4]. Last but not least, a very high tolerance to ionizing radiations has also been reported [1], arising from the crystallographic structure typical of these MAS ceramics. The latter consists of a FCC close-packed oxygen sublattice, with cations Mg^{2+} and Al^{3+} occupying respectively tetrahedral and octahedral interstitial sites. The cations occupy only partially these sites (1/2 or Al^{3+} and 1/8 for Mg^{2+}) allowing their displacement under irradiation within the lattice while the charge equilibrium is conserved. Hence damage is reduced [1,2]. Due to its peculiar lattice, spinel structure can exhibit several defects, from the anti-site defects (Mg^{2+} and Al^{3+} exchanging places) to the vacancies (F type centres or oxygen vacancies, and V type centres or cationic vacancies) [5–7]. These defects have huge influences on the physical properties of the materials, hence the understanding of their nucleation and annihilation as function of the fabrication process is of high importance, and requires pertinent experimental techniques. Recent works have shown that luminescence and electronic paramagnetic resonance spectroscopies are quantitative probes of the population of different defects [8,9]. The aim of this article is to follow the evolution of structural defects in fine-grain $MgAl_2O_4$ ceramics following consolidation of spinel powders via Spark Plasma Sintering (SPS) and heat treatment under air.

2 Materials and methods

Sintered samples have been obtained by using a commercial MAS powder from Sasol GmbH, Germany, with particle diameters in between 20 to 50 μm. The powder show impurity content below 5 ppm and more details can be found in our previous work [8]. Sintering was car-

[a] e-mail: hugo.spiridigliozzi@lspm.cnrs.fr (corresponding author)

ried out using the SPS process (Dr. Sinter, LAB Series SPS-515S, Japan), with the same experimental procedure detailed in [8]. The sintering scheme consisted in a first dwell at 600 °C for 10 min to evacuate moisture, while a pressure of 80 MPa was applied, then the temperature of 1500 °C was reached with a heating rate of 100 °C/min, and was maintained for 3 min. The system was cooled afterward with a rate of 100 °C/min, and the pressure released simultaneously. Heat treatments after the densification were realized in a muffle furnace, under air atmosphere. Several temperatures and durations of treatment were tested, but only samples treated at 1100 °C, 1150 °C and 1250 °C for 200 h are analysed here. As a matter of fact, temperatures lower than 1100 °C have shown small annealing effect and durations shorter than 200 h were clearly not enough for observing annealing results throughout the whole thickness of the samples. To characterize the microstructure of the pellets, SEM (ZEISS GEMINI SUPRA^{TM} 40 VP FEG-SEM) was used at partial vacuum of 15 Pa. XRD analysis was carried out using an INEL EQUINOX 1000, with a Co-Kα source, to determine phase composition and crystal structure. A cathode-luminescence (CL) set-up operating at 5K was used to characterize the optical properties, after the deposition of a 3 nm platinum coating onto the sample to avoid surface charging. Detailed description of the set-up can be found in [9]. CL spectra were normalized with respect to the intensity of the Cr^{3+} peak expected to be constant through the process. The microscopic detection and characterization of magnetic sites was performed using conventional X-band (9.47 GHz) Electron Paramagnetic Resonance (EPR) spectroscopy at room temperature (Bruker EMX spectrometer with a TE_{102} resonant cavity).

3 Results

The Rietveld refinement of the XRD patterns (Fig. 1) confirms the spinel structure and reveals that the powder is composed of crystallites of about 155(5) nm with a cell parameter $a = 8.0932(4)$ Å. A contamination by ~ 3 wt% with free MgO periclase phase is also observed. These results are in agreement with our previous studies [8]. Neither change of the cell parameter nor of the composition is observed after sintering and post-densification heat treatment. However, after sintering, peaks are narrower indicating bigger crystallite size and thus confirming the growth effect of the heat treatment.

The SEM images in Fig. 2b shows that the Sasol powder is constituted of agglomerated particles of complex shape, with apparent size d≈20 μ m. After sintering with the scheme described in the experimental section, a transparent pellet was obtained, as shown in Fig. 2a, with the mean grain size $G = 2.9\mu$m (Fig. 2b). A subsequent heat treatments at 1100°C and 1150°C did not lead to the grain coarsening (see Fig. 2b), but heat treatment at 1250 °C induced a grain growth up to a size of $d \approx 4.8\mu$m. The ceramics obtained without post-treatment (called SPSed) presented a strong dark discoloration, which can be attributed to both carbon contamination and partial reduction of $MgAl_2O_4$ during sintering process [10–12]; post-annealing under air can suppress or decrease this phenomenon by re-oxygenation of the O_2^- vacancies and oxidation of the entrapped carbon [13]. Accordingly, after ceramics heat treatment at 1100 °C only a slight lightening is observed, indicating an annealing success only on the surface of the material. In fact, the temperature seems to be still insufficient for the diffusion of oxygen throughout the thickness of the pellet. With a heat treatment at 1150 °C, no darkening remained, but a yellow tint appeared, and the material transparency decreased to translucency. Finally at 1250 °C, the ceramic was white and totally opaque. The decrease of transparency observed in our study has been previously reported in Ref. [13], where the recombination of vacancies leading to a new porosity has been invoked. By microscopic analysis we can also observe blistering at the surface after annealing (not shown here) that seemingly comes from the oxidation of carbon into CO_2 causing high strain and local porosity after the gas evacuation from solids.

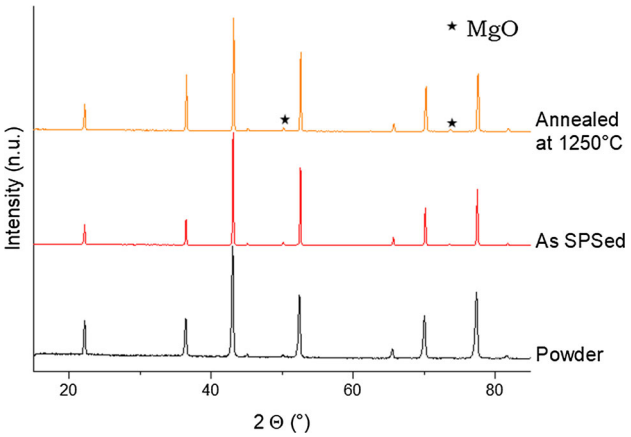

Fig. 1 Peaks marked with a star are from the periclase phase (MgO), unmarked peaks are from the spinel phase ($MgAl_2O_4$)

The cathodoluminescence spectra in Fig. 3 exhibit four main peaks: one at 1.8 eV (not shown) due to Cr^{3+} cation impurities [8,14–16], one at 2.4 eV due to Mn^{2+} cations impurities [8,14,15], and two broad bands at ~ 3.4 eV and ~ 5.2 eV respectively attributed to F-type centres [6,20–22] and cationic disorder including inversion defects and V-type centres [7,15,20]. Note that the latter two broad peaks are the convolution of several bands, as it has been previously reported [6,20–22] and as can be clearly seen in the case of the CL spectrum for the annealed sample at 1250 °C (Fig. 3, orange line). In this case, in fact, the overall 3.4 eV band intensity is highly reduced by the heat treatment and the 3.3 eV peak linked to a "harder to anneal" F-type defects clearly appeared. Also, a minor peak appeared at 2.55 eV after annealing at 1150 °C. This peak can be

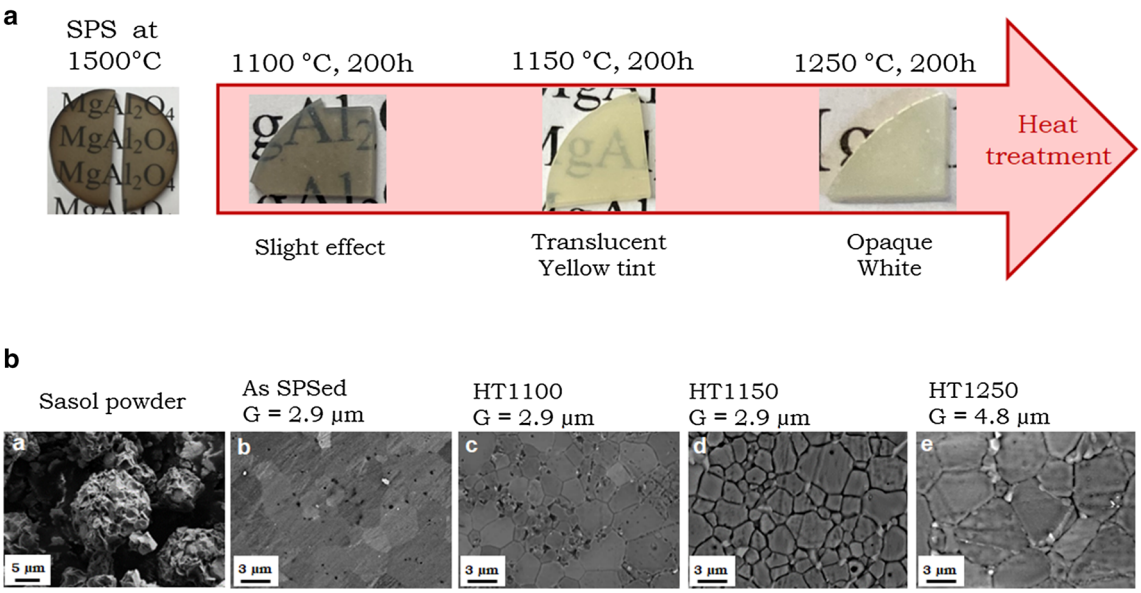

Fig. 2 Images of the sintered ceramics with their fabrication process parameters showing the evolution of the transparency of the pellets (**a**) and SEM images of studied samples: from the powder to the different sintered materials (**b**)

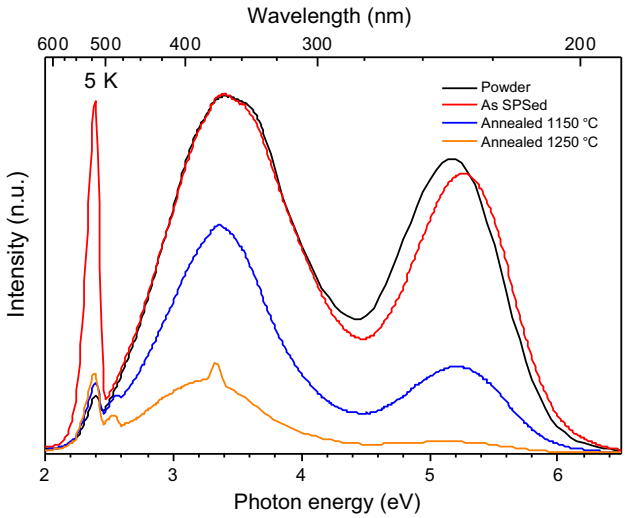

Fig. 3 Cathodoluminescence spectra for all samples: from the powder to the whole sintered sample under different fabrication conditions

attributed to the luminescence band of the agglomerate F2 centre (i.e. the combination of two F centres) [22], which is in good agreement with the mechanism proposed in [13], leading to new porosity after heat treatment and explaining the loss of transparency (see Fig. 2a).

The Cr and Mn impurities come from the powder and, of course, they cannot be suppressed during the applied fabrication process. Besides Cr can only be in the Cr^{3+} valence state in the MAO, this is the reason why we normalized all the CL spectra to the intensity of the 1.8 eV peak, which is not expected to evolve depending on the fabrication conditions. However, the intensity of the signal peaking at 2.4 eV was significantly different at each step of the treatment, indicating a modification of the oxidation state of Mn. More specifically, the intensity of this peak is multiplied by a factor of 6 from the powder to as-SPSed ceramic. This can be explained by the reductive atmosphere used during the sintering process and thus converting Mn^{4+} ions (in an octahedral site, substituting the Al^{3+}) into Mn^{2+} (in a tetrahedral site, substituting the Mg^{2+}). After the annealing under air (oxidizing atmosphere), the 2.4 eV peak intensity decreased back to almost the same level of intensity obtained for the powder. Such conversion of the Mn oxidation state has already been reported in several oxides, both after sintering [17] and after post-densification annealing [18,19]. CL spectra in Fig. 3 evidenced that SPS process does not affect the luminescence of F-type centres at 3.4 eV, although it was expected to have the greatest influence on this band, due to partial reduction of MAS and formation of new oxygen vacancies. The already high concentration of F-centres in the raw powder may explain the fact that no further reduction of spinel was observed; since the O^{2-} vacancies density did not evolve after SPS, the dark discoloration of the material afterward (Fig. 2a) is most likely not due to these defects. However, luminescence of V-type centres at 5.5 eV underwent a blue shift, which indicates a change of the cationic defects (possibly via inversion) and emphasizes a complex nature of this band. The luminescence of F and V centres decreased greatly after the heat treatment, which can be interpreted as a healing of structural defects, and which is corroborated by a progressive change of the coloration from black to white (observed in Fig. 2a). At 1250 °C, there remained almost no V-type centres in the material and the sample was fully opaque white; these defects, while not being its primary cause, may be partly responsible for the discoloration, in particu-

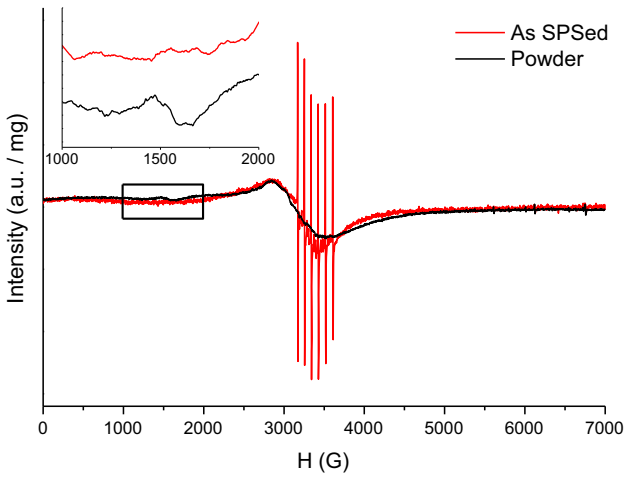

Fig. 4 EPR spectra at room temperature using a 9.47 GHz conventional X-band spectrometer. Inset zooms on a square in EPR spectrum

Table 1 Mean resonance fields (H) obtained after Gaussian fit of EPR spectra in $MgAl_2O_4$ powder and SPS ceramics

Sample	H (G)		
	BS2	BS1	HFS
Powder	1542 G	3175 G	–
Ceramics	–	3158 G	3384 G

lar for the yellow tint remaining after heat treatment at 1150°C.

The EPR spectroscopy was carried out on two samples: powder and pellet obtained after SPS process without any heat treatment, and the obtained spectra are presented in Fig. 4. Three main signals can be observed on the spectra (see Table 1):

(i) Hyperfine structure (HFS) sextet with mean resonance field H =3384 G ($g = 2.00 \pm 0.02$), attributed to the Mn^{2+} cations [23–25],
(ii) Broad signal (BS1) around the mean resonance field H =3175 G (g = 2.13) and H =3158 G (g =2.14) in respectively powder and ceramics, which can be attributed to overlapping signals from several structural defects (F-type centres [6,10,24,26,28] and V-type centres [6,7,27]) and confirms the CL results,
(iii) Broad signal of weak intensity (BS2) at H =1542 G (g =4.39), which has been previously assigned to isolated cations located at distorted sites (V-centres) [6] or, alternatively, to Fe^{3+} impurities [28].

We notice that the existing hypotheses about BS2 nature cannot be admitted, since this signal disappeared in our experiments after powder sintering. We therefore tentatively ascribe it to Mn^{4+} cations by analogy with what was previously reported in $Lu_3Al_5O_{12}$ [19] and in $PbTiO_3$ [17]. This hypothesis is in a good agreement with our measured CL spectra (Fig. 3) showing an increase of Mn^{2+} intensity after SPS. In agreement, BS2 signal is not visible anymore after sintering while HFS sextet of Mn^{2+} appeared. Further EPR measurements of the annealed samples after sintering will clarify the origin of BS2 signal; this work is under way. We notice that the Mn^{4+} ions are known to exhibit in $MgAl_2O_4$ spinel a broadband luminescence at 651 nm (1.90 eV) associated with the parity and spin-forbidden $^2E_g \rightarrow {}^4A_{2g}$ transition [29]. Although this luminescence is expected to be low, future careful analysis of the NIR spectral region could provide valuable information about the $Mn^{4+} \rightarrow Mn^{2+}$ exchange. It is interesting to underline that the BS1 signal is not strongly altered after sintering, which is also in good agreement with CL results showing that the F-type and V-type centres undergo little change from the powder to the as-SPSed ceramic. Hence, the applied sintering does not have a strong effect on structural defects in $MgAl_2O_4$ spinel, in spite of what is commonly accepted.

4 Conclusions

In this study we analysed the effect of powder consolidation via SPS process and subsequent thermal annealing treatments under air on microstructural properties and transparency of $MgAl_2O_4$ ceramics. We showed that CL and EPR spectroscopies allow constructing a cogent picture for the presence of impurities and also for the evolution of the recombination centres effects as function of the fabrication process. An interesting feature is that the sintering technique does not have a strong effect on the structural defects and thus this means that defects are mostly present in the precursor powder in our case. The dark discoloration induced by SPS process is mainly due to carbon contamination and can be effectively inhibited via post-annealing under air, as well as V and F type centres, to the detriment of transparency.

Acknowledgements This work has been carried out within the framework of the EUROfusion Consortium, funded by the European Union via the Euratom Research and Training Programme (Grant Agreement No 101052200—EUROfusion). Views and opinions expressed are however those of the author(s) only and do not necessarily reflect those of the European Union or the European Commission. Neither the European Union nor the European Commission can be held responsible for them. The authors are grateful to the SPS Platform Ile-de-France (France) and would like to thank B. Villeroy (ICMPE-CNRS, France) for his technical expertise.

References

1. K.E. Sickafus et al., Science **289**(5480), 748–751 (2000). https://doi.org/10.1126/science.289.5480.748

2. K.E. Sickafus et al., Nucl. Instrum. Methods Phys. Res. Sect. B Beam Interact. Mater. Atoms **106**, 573–578 (1995). https://doi.org/10.1016/0168-583X(95)00772-5
3. A. Goldstein, J. Eur. Ceram. Soc. **32**(11), 2869–2886 (2012). https://doi.org/10.1016/j.jeurceramsoc.2012.02.051
4. I. Ganesh, Int. Mater. Rev. **58**(2), 63–112 (2013). https://doi.org/10.1179/1743280412Y.0000000001
5. Q. Li et al., J. Phys. Chem. Solids **145**, 109542 (2020). https://doi.org/10.1016/j.jpcs.2020.109542
6. Savita et al., J. Appl. Phys. **129**(12), 125111 (2021). https://doi.org/10.1063/5.0045385
7. A. Lushchik et al., Nucl. Instrum. Methods Phys. Res. Sect. B Beam Interact. Mater. Atoms **435**, 31–37 (2018). https://doi.org/10.1016/j.nimb.2017.10.018
8. A. Pille et al., Ceram. Int. **45**(7), 8305–8312 (2019). https://doi.org/10.1016/j.ceramint.2019.01.137
9. E. Feldbach et al., Opt. Mater. (Amst) **55**, 164–167 (2016). https://doi.org/10.1016/j.optmat.2016.03.008
10. K. Morita et al., J. Ceram. Soc. Jpn. **123**(1442), 983–988 (2015). https://doi.org/10.2109/jcersj2.123.983
11. K. Morita et al., Acta Mater. **84**, 9–19 (2015). https://doi.org/10.1016/j.actamat.2014.10.030
12. H. Hammoud et al., Ceramics **2**(4), 612–619 (2019). https://doi.org/10.3390/ceramics2040048
13. P. Fu et al., Opt. Mater. (Amst) **36**(7), 1232–1237 (2014). https://doi.org/10.1016/j.optmat.2014.02.035
14. E. Feldbach et al., Opt. Mater. (Amst) **96**, 109308 (2019). https://doi.org/10.1016/j.optmat.2019.109308
15. G. Prieditis et al., IOP Conf. Ser. Mater. Sci. Eng. **503**(1), 012021 (2019). https://doi.org/10.1088/1757-899X/503/1/012021
16. M.G. Brik et al., J. Lumin. **177**, 145–151 (2016). https://doi.org/10.1016/j.jlumin.2016.04.043
17. D. Ramírez-Rosales et al., Solid State Commun. **118**(7), 371–376 (2001). https://doi.org/10.1016/S0038-1098(01)00072-2
18. V. Amir-Ebrahimi, J.J. Rooney, J. Mol. Catal. A Chem. **159**(2), 429–432 (2000). https://doi.org/10.1016/S1381-1169(00)00208-9
19. Y. Zhang et al., Opt. Mater. (Amst) **101**, 109705 (2020). https://doi.org/10.1016/j.optmat.2020.109705
20. E. Feldbach et al., Opt. Mater. (Amst) **96**, 109308 (2019). https://doi.org/10.1016/j.optmat.2019.109308
21. S. Sawai, T. Uchino, J. Appl. Phys. **112**(10), 103523 (2012). https://doi.org/10.1063/1.4767228
22. D. Valiev et al., Opt. Mater. (Amst) **91**, 396–400 (2019). https://doi.org/10.1016/j.optmat.2019.03.049
23. A.F. Zatsepin, J. Alloys Compd. **834**, 154993 (2020). https://doi.org/10.1016/j.jallcom.2020.154993
24. Y. Wakui et al., Mater. Res. Bull. **90**, 51–58 (2017). https://doi.org/10.1016/j.materresbull.2017.02.001
25. J.S. Shaffer et al., Phys. Rev. B **13**(5), 1869–1875 (1976). https://doi.org/10.1103/PhysRevB.13.1869
26. N. Mironova-Ulmane et al., Radiat. Meas. **90**, 122–126 (2016). https://doi.org/10.1016/j.radmeas.2015.12.020
27. A. Ibarra et al., Phys. Rev. B **44**(14), 7256–7262 (1991). https://doi.org/10.1103/PhysRevB.44.7256
28. V.A. Dutov et al., AIP Conf. Proc. **2174**, 020097 (2019). https://doi.org/10.1063/1.5134248
29. H. Ji et al., Dalton Trans. **49**, 5711–5721 (2020). https://doi.org/10.1039/D0DT00931H